Received: 28 June 2019 | Accepted: 10 January 2020

DOI: 10.1002/vzj2.20015

Vadose Zone Journal

ORIGINAL RESEARCH ARTICLE

# Heterogeneity of the peat profile and its role in unsaturated sodium chloride rise at field and laboratory scales

**Nicole E. Balliston** | **Jonathan S. Price**

Dep. of Geography and Environmental Management, Univ. of Waterloo, Waterloo, ON, N2L 3G1, Canada

**Correspondence**
Nicole E. Balliston, Dep. of Geography and Environmental Management, Univ. of Waterloo, Waterloo, ON, N2L 3G1, Canada.
Email: nballist@uwaterloo.ca

**Funding information**
Canada First Research Excellence Fund (CFREF) Global Water Futures, Grant/Award Number: 2007922

**Abstract**

Resource extraction in Canada's boreal ecozone increases the risk of contaminant release into the area's extensive bog and fen peatlands. Lateral spreading, then upwards transport of solutes into the vadose zone of these moss-dominated ecosystems, could be toxic to vegetation. To evaluate the rate and character of contaminant rise in a subarctic bog, vadose zone-specific conductance and water content were measured in four hummocks ~5 m downslope of a 45-d 300-mg $L^{-1}$ NaCl release. Four 30-cm-deep hummock peat mesocosms were extracted adjacent to the release site for an unsaturated evaporation-driven NaCl breakthrough experiment and subsequent parameterization. The field rate of solute accumulation was slower in near-surface (0–5 cm) peat, where low water contents limited pore connectivity. Solute accumulation was reduced by downward flushing by rain, though this was lesser in near surface moss where solute remained held in small disconnected pores. In the laboratory, $Cl^-$ rise reached the 15-cm depth in all mesocosms by Day 65. Sodium rise was 2.2 times slower, likely due to adsorption to the peat matrix. Rates of upwards solute movement were highly variable; the highest rates occurred in the mesocosm with small but hydrologically conductive pores near the surface, and the lowest occurred where vascular roots disrupted the physical structure of the peat. This research demonstrates that solute spilled into a bog peatland is likely to rise and be retained in the vadose zone. However, hydraulic and solute transport behaviors are sensitive to the vertical structure of peat, underscoring the need for extensive sampling and parameter characterization.

## 1 | INTRODUCTION

Increasing extraction and transportation of mineral resources in the boreal zone of Canada poses a risk of contaminant release into bog and fen peatlands, which dominate the subarctic landscape (Riley, 2011). Contaminant releases can be unintentional (e.g., leakage from pipelines or spills via train derailment; Zoltai & Kershaw, 1995) or intentional (e.g., wastewater from mining camps; Steinback, 2012). Once released into these systems, there is potential for downgradient solute migration (Baird & Gaffney, 2000; Balliston, McCarter, & Price, 2018; Hoag & Price, 1995; McCarter & Price, 2017a), accumulation within the variably saturated upper zone (Simhayov, Weber, & Price, 2018), and in some cases vertical smearing due to water table fluctuations (Dobson, Schroth, & Zeyer, 2007; Gharedaghloo & Price,

**Abbreviations:** awt, above water table; bgs, below ground surface; PVC, polyvinyl chloride; TDR, time domain reflectometry.

2018). This has potential toxicity to vascular and nonvascular plants (Pouliot, Rochefort, & Graf, 2012; Rezanezhad, Price, & Craig, 2012). Contaminant redistribution within the variably saturated upper zone, in particular solute movement and accumulation due to capillary action (McCarter & Price, 2014; Price & Whittington, 2010), has received little attention and remains poorly understood, especially in undisturbed *Sphagnum* peat profiles.

The upper, variably saturated layer of the peat soil profile, known as the acrotelm (Ingram, 1978), is composed of living vegetation and relatively poorly decomposed organic material. It has a network of relatively large, open, and connected pores that readily transmit flow under saturated conditions (Goetz & Price, 2015; McCarter & Price, 2014; Rezanezhad et al., 2010; 2016). However, this upper layer drains readily when the water table drops, causing a decrease in unsaturated hydraulic conductivity of up to five orders of magnitude with increasingly negative pore water pressure (Price et al., 2008). The transition from acrotelm to the perpetually saturated catotelm (Ingram, 1978) is marked by an increasing degree of decomposition (Hayward & Clymo, 1982) and soil compaction (Quinton, Elliot, Price, Rezanezhad, & Heck, 2009). Deeper in the acrotelm, the more decomposed peat has a higher water retention capacity, and thus higher unsaturated hydraulic conductivity at a given negative pressure, compared with acrotelm peat (Price et al., 2008). A gradual transition in soil hydraulic properties from the lower to upper acrotelm provides good vertical connectivity that can sustain water rise, though this may also enhance loss to evapotranspiration (Gauthier, McCarter, & Price, 2018; McCarter & Price, 2014; Nungesser, 2003).

Upwards movement of water in the unsaturated zone has the potential to transmit dissolved solutes within the open, well-connected "active" pore spaces. However, its passage can be slowed when solutes diffuse from this mobile fluid into closed and dead-end pore spaces (Hoag & Price, 1997; McCarter & Price, 2017b; McCarter, Rezanezhad, Gharedaghloo, Price, & Van Cappellen, 2019; Rezanezhad et al., 2012; Ronkanen & Kløve, 2007) common in *Sphagnum* peat (Hayward & Clymo, 1982; Lewis, 1988). Reactive solutes such as cations may further accumulate as they adsorb to the peat (Simhayov et al., 2018; McCarter & Price, 2017b; Rezanezhad et al., 2012, 2016).

The movement and accumulation of solute above the water table in natural peat, at both laboratory and field scales, is not well documented. Solute breakthrough experiments have been conducted under saturated conditions (Hoag & Price, 1997; Ours, Siegel, & Glaser, 1997; Price & Woo, 1986; Rezanezhad et al., 2012); however, to our knowledge, only one transport experiment has been executed in an unsaturated peat column (Simhayov et al., 2018). That unsaturated transport experiment used homogenized, moderately decomposed fen peat with the large inclusions removed, so it does not represent the layered heterogeneity of a natural peat profile that is so important to peatland hydrology (Waddington et al., 2015). Moreover, the peat used by Simhayov et al. (2018) was sufficiently degraded that it did not exhibit the dual porosity transport behavior commonly reported for *Sphagnum*-dominated peat (Weber, Iden, & Durner, 2017). Therefore, the purpose of this research is to better understand the potential for solutes, and in particular NaCl, in the saturated zone to migrate to the living, growing surface of *Sphagnum* peat profiles, based on their characteristic hydraulic structure and ambient conditions. The specific objectives are to

1. Determine the ability of *Sphagnum* hummocks to accumulate and retain NaCl above the water table under field conditions and relate solute accumulation to depth and variability of the water table, and volumetric soil water content;
2. Assess the vertical rise of NaCl in *Sphagnum* mesocosms taken from the field site, under controlled steady-state laboratory conditions, to observe the nature and rate of solute redistribution within an undisturbed peat profile; and
3. Examine depth-dependent hydrophysical properties and their heterogeneity between and within mesocosms, and relate them to rates and patterns of NaCl accumulation in unsaturated conditions.

**Core Ideas**

- There is a high potential for solute uplift in unsaturated subarctic bog peat.
- Hydrophysical properties are highly variable in shallow moss-dominant bog peat.
- Solute is held above the water table where pores are small and disconnected.

## 2 | MATERIALS AND METHODS

### 2.1 | Study site

The study site is a 4,500-$m^2$ area located in the James Bay lowlands (Figure 1), northwest of the De Beers Group of Companies' Victor Mine (51°51′13″ N, 83°56′26″ W; 85 m asl). It is on the margin of a continental domed bog, which gently slopes towards a stream; the sitewide gradient is ~0.004 m $m^{-1}$. The site extent is defined by the final shape of a NaCl plume generated during a 45-d continuous solute release experiment (Balliston et al., 2018). There is a distinct hummock and hollow microtopography formed by *Sphagnum* mosses. The

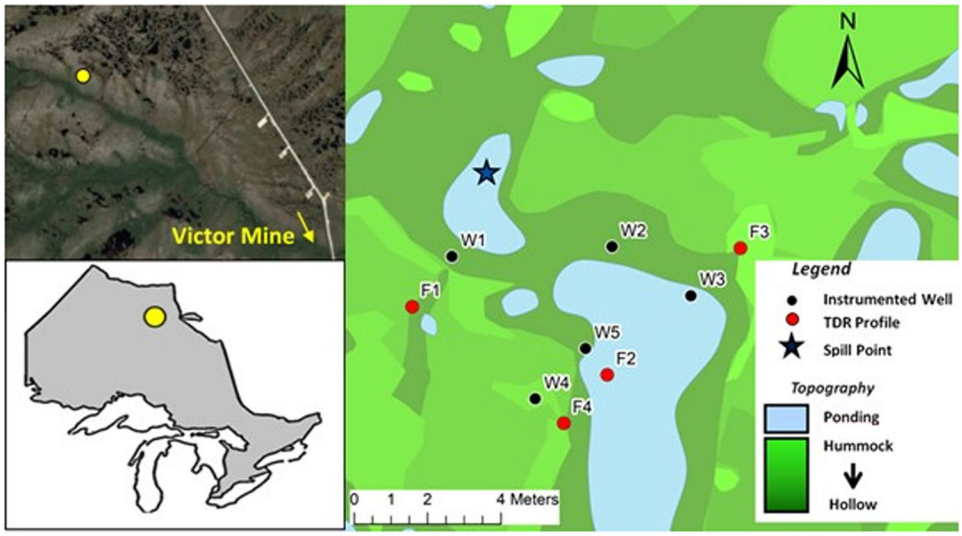


**FIGURE 1** Location of the study site in the James Bay lowlands (bottom left) relative to the De Beers Group of Companies Victor Diamond Mine (top left). Site microtopography and well and time domain reflectometry (TDR) installations are also shown (right)

hummocks are composed mainly of *Sphagnum fuscum* (Schimp.) Klinggr. and are typically 0.5–1.0 m in diameter and 10–15 cm high. Stunted 1- to 4-m-tall *Picea mariana* (Mill.) Britton., Sterns & Poggenb. (black spruce) trees are found scattered throughout the site. Peat thickness varies between 1.25 and 2.15 m. Average January and July temperatures (1981–2010 climate normals) are −20.7 and 15.4 °C at Moosonee (250 km southeast), and −22.4 and 17.1 °C at Lansdowne House (300 km southwest), and average annual precipitation is 700 and 681 mm, respectively, with 30 and 35% falling as snow (Environment Canada, 2015a, 2015b).

## 2.2 | Field experiment

Vadose zone field data were collected during a 45-d solute injection experiment conducted at the site in 2015 between 5 July (Day 0) and 18 August (Day 45). Sodium chloride was used as the solute tracer due to its low reactivity, ease of in-field measurement through the surrogate measure of specific conductance (SC) (Hoag & Price, 1995), and low background concentrations. The implications of $Na^+$ adsorption are discussed below. Diluted NaCl was injected into a fully penetrating well 1.5 m below ground surface (m bgs), at an average flow rate of 13,500 L $d^{-1}$, and an average NaCl mass flux of 2.7 kg $d^{-1}$. Average $Cl^-$ and $Na^+$ concentrations were 182 and 118 mg $L^{-1}$, respectively, and average specific conductance was 543 μS $cm^{-1}$ (a more detailed explanation of the injection system is described by Balliston et al., 2018).

Specific conductivity (SC) was used as a proxy to evaluate solute movement in the saturated and unsaturated zones; four hummocks (F1–F4) within 10 m of the injection point were instrumented with three Campbell Scientific CS 615 probes connected to a time domain reflectometer (Campbell Scientific TDR 100, Figure 1). Probes were installed 5, 10, and 15 cm bgs of each hummock. Bulk SC and dielectric constant ($K_a$) data were recorded using these probes every 20 min on a Campbell Scientific CR1000 logger. Water content (θ) was determined given the $K_a$ values using the calibration for peat outlined by Kellner and Lundin (2001). Bulk SC values were corrected for θ to determine porewater SC using the method outlined in Hilhorst (2000).

Saturated zone SC and water temperature data were collected from five 2.54-cm i.d. polyvinyl chloride (PVC) wells (W1–W5 in Figure 1) that were sealed at the bottom but slotted over a 1.25-m interval, screened with geotextile filter sock (Rice Engineering & Operating, 2-inch[5.1-cm] filter sock). Water temperature and water level were recorded at 30-min intervals using Schlumberger Mini-Diver D1501 pressure transducers installed in W1–W5. Specific conductance values were recorded in W1, W3, and W4 at 30-min intervals using Hobo U24 conductivity data loggers. Manual measurements of water temperature and SC were also taken at W1–W5 and compared with logged results to ensure consistent logging accuracy.

Precipitation totals and evaporative fluxes were determined using the methods of Balliston et al. (2018).

## 2.3 | Unsaturated solute breakthrough experiment

For laboratory experiments, four peat mesocosms (L1–L4) were collected in 23-L buckets from hummocks directly north of the site (uncontaminated), all within a 5-m radius, representing the upper 30 cm of the peat profile including the living

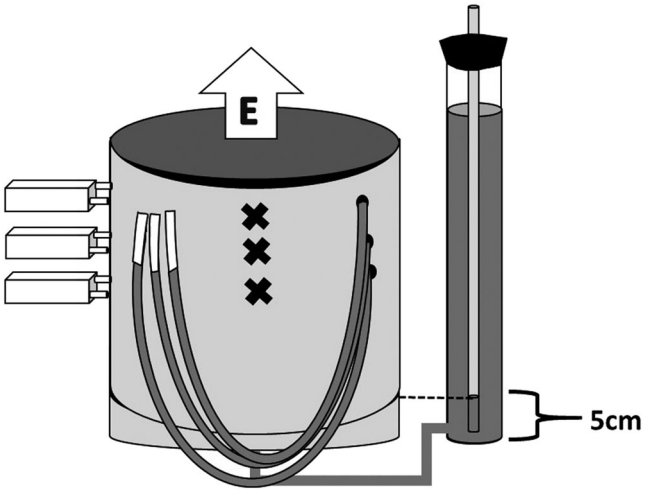


**FIGURE 2** Schematic of the setup used in the unsaturated solute breakthrough experiment. The bottom outlet of each mesocosm was connected to a Marriot system (far right) that maintained the water table 5 cm above the bottom. Cores were left open to facilitate evaporation (E). Three CS 615 probes (far left) and three tensiometers (right side of mesocosm) were installed at 5, 10, and 15 cm below ground surface (bgs) to measure specific conductivity (SC) and water content (θ), and water pressure, respectively. Three sampling ports (middle of mesocosm − crosses) were installed at 7.5, 12.5, and 17.5 cm bgs for biweekly sample extraction

vegetation (surficial non-moss vegetation was trimmed). The mesocosms were frozen for preservation prior to shipment and refrozen upon arrival at the laboratory to prevent decomposition. Each mesocosm was then shaved while frozen, to tightly fit into a 25-cm i.d. PVC conduit, sealed at the bottom to prevent leakage, with a spigot for water supply. These mesocosms were used to test and simulate the capillary rise of solutes into the unsaturated zone under controlled conditions.

For the duration of the experiment, the four mesocosms were bolted to platforms in a climate-controlled room with a temperature of 26.5 ± 1.7 °C and relative humidity of 35 ± 3%. The bottom outlet of each mesocosm was connected to a Marriot system to supply water and solute for evapotranspiration and to hold the water table in the mesocosm 5 cm above its bottom (Figure 2).

Each mesocosm was outfitted with Campbell Scientific CS 615 probes at 5, 10, and 15 cm bgs for the measurement of bulk SC and θ, at 5-min intervals. The probe lengths were 30 cm, whereas the diameter of the mesocosm was 25 cm, leaving 5 cm of probe outside of the mesocosm. To account for this, a correction factor was applied to the $K_a$ data before being converted to θ using Equation 1 (Whittington & Martin, personal communication, 2014):

$$\frac{\log(K_{a2}) - \log\left(K_{a1}\right)}{l_2 - l_1} = 0.029 \quad (1)$$

where $K_{a1}$ and $K_{a2}$ are the measured and corrected dielectric constants (–), and $l_1$ and $l_2$ are the actual inserted probe length (25 cm) and the fully inserted probe length (30 cm), respectively. Values of bulk SC were corrected for θ to porewater SC using Hilhorst (2000).

Tensiometers comprising a porous clay cup and flexible silicon tube open to the atmosphere were installed at 5, 10, and 15 cm bgs for daily manual measurement of matric pressure. Small pans of water were placed adjacent to the top of each mesocosm and weighed daily to determine the difference in evaporative rates as a function of mesocosm placement in the room. Sampling occurred 1 d before solute introduction and biweekly thereafter. Porewater was extracted using 5-cm-long porous ceramic sampling tubes of 2.5-mm diam. (19.21.05, Rhizon, Rhizonsphere) connected to a syringe dedicated to each port, which collected a sample over a 12-h period using consistently applied suction. Sampling ports were installed 2.5 cm below each TDR probe to extract 5–10 ml of porewater for anion and cation analysis without disrupting the measurement of SC and $K_a$. Prior to sample collection, each syringe was purged three times with ultrapure water (18.2 MΩ cm). One duplicate sample was collected for every 10 samples collected, to test for reproducibility. Chloride and $Na^+$ concentrations were analyzed at the University of Waterloo Biogeochemistry laboratory using a Thermo Scientific Dionex ion chromatograph.

Prior to the start, each mesocosm was flushed slowly from the bottom with one pore volume of 300 mg $L^{-1}$ NaCl solution (182 and 118 mg $L^{-1}$ of $Cl^-$ and $Na^+$, respectively), followed by a minimum of five pore volumes of ultrapure water. This was done to mitigate pore dilation or clogging caused by changes in ionic strength of the solution (McCarter, Weber, & Price, 2018) in later breakthrough tests. Ultrapure water was then added to each Marriot tube and the system was left for 60 d at a water level of 25 cm bgs to minimize subsidence during the experimental period and to achieve steady-state evaporative conditions. At 1200 h on Day 0 of the solute breakthrough experiment, a 300-mg $L^{-1}$ NaCl solution was added to the Marriot system in cores L1, L2, and L3. Mesocosm L4 was used as a control for background conditions and thus did not receive NaCl. To prevent stratification, the solute within the Marriot tube was mixed for 5 min every hour using a timed low-flow 12-V mini water pump. The experiment duration was 66 d from the time of initial NaCl addition. Fluid level in the Marriot system was measured daily with a measuring tape and refilled as necessary.

After the experiment, simple linear regression (95% confidence interval) was performed on the porewater SC and $Cl^-$ and $Na^+$ concentrations measured above the detection limit. Statistically significant correlations at the 95% confidence interval were used to transform SC into $Cl^-$ and $Na^+$ concentrations using the equation of the fitted line (Supplemental Table S1).

## 2.4 | Physical soil properties

After the solute breakthrough experiment was complete, each mesocosm was flushed repeatedly with ultrapure water until the outflow conductivity reached background values. Each mesocosm was then subdivided into two subcores (A and B) of 10-cm diam. and sliced into 5-cm vertical sections for soil property analysis.

Water retention and unsaturated hydraulic conductivity ($K_{unsat}$) were determined for each 5-cm mesocosm slice at increasingly negative pressure steps (−5, −10, −15, and −25 cm) using the tension disk method outlined by (McCarter & Price, 2017b). Hydraulic conductivity and slice mass were measured for each pressure step and curves for $K_{unsat}$ and θ were generated as a function of soil water pressure (ψ). The equivalent saturated pore size for each pressure step was determined using the capillary rise equation (Bear, 1972)

$$r = \frac{2\gamma cps\beta}{\rho g h} \tag{2}$$

where $r$ is the theoretical pore opening radius (m), γ is the surface tension of water (N m$^{-1}$), β is the contact angle (51° for near-surface peat; Gharedaghloo & Price, 2018), ρ is the density of water (kg m$^{-3}$), $g$ is gravitational acceleration (m s$^{-2}$), and $h$ is pressure head (m). The fraction of water filled pores is

$$\emptyset_{vw} = \frac{\theta(\psi)}{n_T} \tag{3}$$

where θ is the water content (–) at pressure ψ and $n_T$ is the total porosity (–). The fraction of pores at each pressure interval is the difference in the fraction of water-filled pores at consecutive pressure steps, which was used to generate pore size distributions for each slice.

The saturated hydraulic conductivity ($K_{sat}$) was measured on each 5-cm slice using a constant head Darcy permeameter test.

Total porosity ($n_t$) was assumed to be the water content at 100% saturation. Volumetric water content was calculated at saturation and for all pressure steps in the $K_{unsat}$ experiment as

$$\theta_\psi = \frac{(M_\psi - M_{dry})}{V_t \rho_w} \tag{4}$$

where $\theta_\psi$ is the volumetric water content at the given pressure condition (–), $M_\psi$ is the mass of the slice at the given pressure condition (g), $M_{dry}$ is the mass of the dry slice (g), $\rho_w$ is the density of water (g cm$^{-3}$), and $V_t$ is the measured sample volume (cm$^3$).

Effective porosity was determined using the pressure plate method outlined by McCarter and Price (2017a), which assumed it was equal to the difference between saturated volumetric water content and that at −100 cm,

$$n_e = \theta_{-100cm} = \frac{(M_{sat} - M_{100cm})}{V_t \rho_w} \tag{5}$$

where $n_e$ (–) is the effective porosity, $M_{sat}$ (g) is the saturated mass of the slice, $M_{-100cm}$ (g) is the mass of the slice at a drainage pressure of −100 cm, $\rho_w$ (g cm$^{-3}$) is the density of water, and $V$ (cm$^3$) is the volume of the section. Specific yield ($S_y$) was calculated using Equation 5, substituting the −100 cm mass for the 24-h atmospheric drained mass.

Sections were dried at 110 °C for 48 h and weighed to determine the dry mass. Saturated and dry bulk densities were calculated by dividing the mass at each respective state by the section volume.

# 3 | RESULTS

## 3.1 | Field experiment

The 2015 field season experienced a wetter summer than average, with a total of 233 mm of precipitation between 5 July and 19 August (Figure 3) compared with the July–August combined climate normal of 175 mm (1981–2010) (Environment Canada, 2015a, 2015b). Evapotranspiration was relatively consistent compared to precipitation, with an average rate of 1.5 ± 0.87 mm d$^{-1}$ (Balliston et al., 2018).

In the saturated zone, the water table was lowest in all hummocks on Day 0 (Figure 3). Significant water table fluctuations correspond to rainfall events on Days 0/1 (17 mm), 7/8 (47 mm), 11/12 (40 mm), and 19/20 (34 mm). In F1, the minimum water table depth (5 cm bgs) was reached during the Day 7 and 19 events, decreasing to ∼10–11 cm bgs between rainfalls. In F2 and F4, water levels peaked at 3 and 17 cm bgs, respectively, during the Day 19 event before declining to 6–8 and 22–24 cm bgs for the rest of the spill. Water table levels fluctuated most in F3; the minimum depth (13 cm bgs) was reached six times between Days 7 and 19, declining quickly between events to 16–18 cm bgs, where it remained stable from Day 27 onwards.

Well SC ($SC_w$) response to rainfall events was variable over the spill duration (Figure 4). Prior to Day 19 (or Day 21 in F3), rainfall events decreased $SC_w$ values, whereas rainfall on and after the Day 19 rainfall events is associated with $SC_w$ spikes.

Over the spill duration, probes F1-5, F3-5, F3-10, F4-5, F4-10, and F4-15 remained unsaturated (Figure 4); the remainder of the probes were not included, as their SC fluctuations reflect saturated zone processes. Temporal variations in θ were relatively consistent with the rise and fall of the water table; the lowest θ on all probes was on Day 0, and the highest was on Day 19, with notable fluctuations after each major

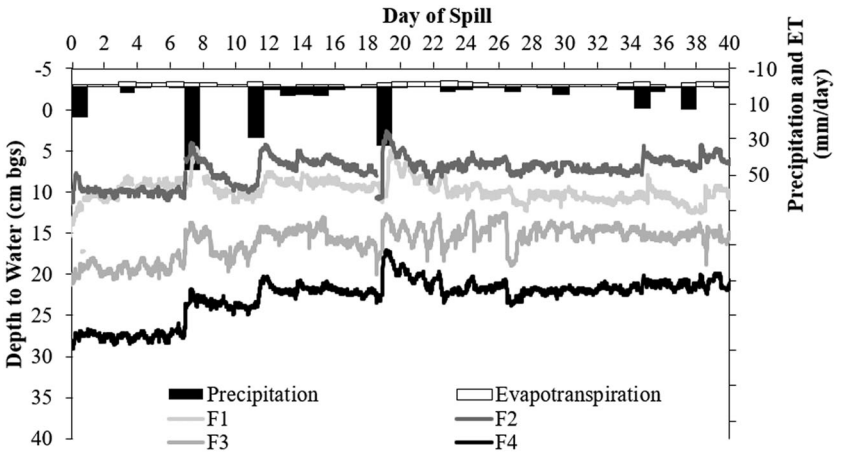


**FIGURE 3** Depth to water table (primary *y* axis, in cm below ground surface [bgs]) and daily precipitation and evapotranspiration (ET, secondary *y* axis) in the vicinity of the instrumented hummocks over the spill duration

rainfall event except in the 0- to 5-cm probes. The degree of θ response to rainfall increased with depth, fluctuating by 2–5% in the 5-cm probes, and ~3–10% in the deeper probes.

Background porewater SC ($SC_{pw}$, initial values in Figure 4) decreased with depth and varied between hummocks, with values of ~400, ~250–400, and ~150–200 μS $cm^{-1}$ at F1, F3, and F4 respectively. In all unsaturated probes, with the exception of F1-5, where $SC_{pw}$ remained constant at background level, $SC_{pw}$ increased between rainfall events and decreased rapidly during rainfall up until the Day 19 event (F1-5). After

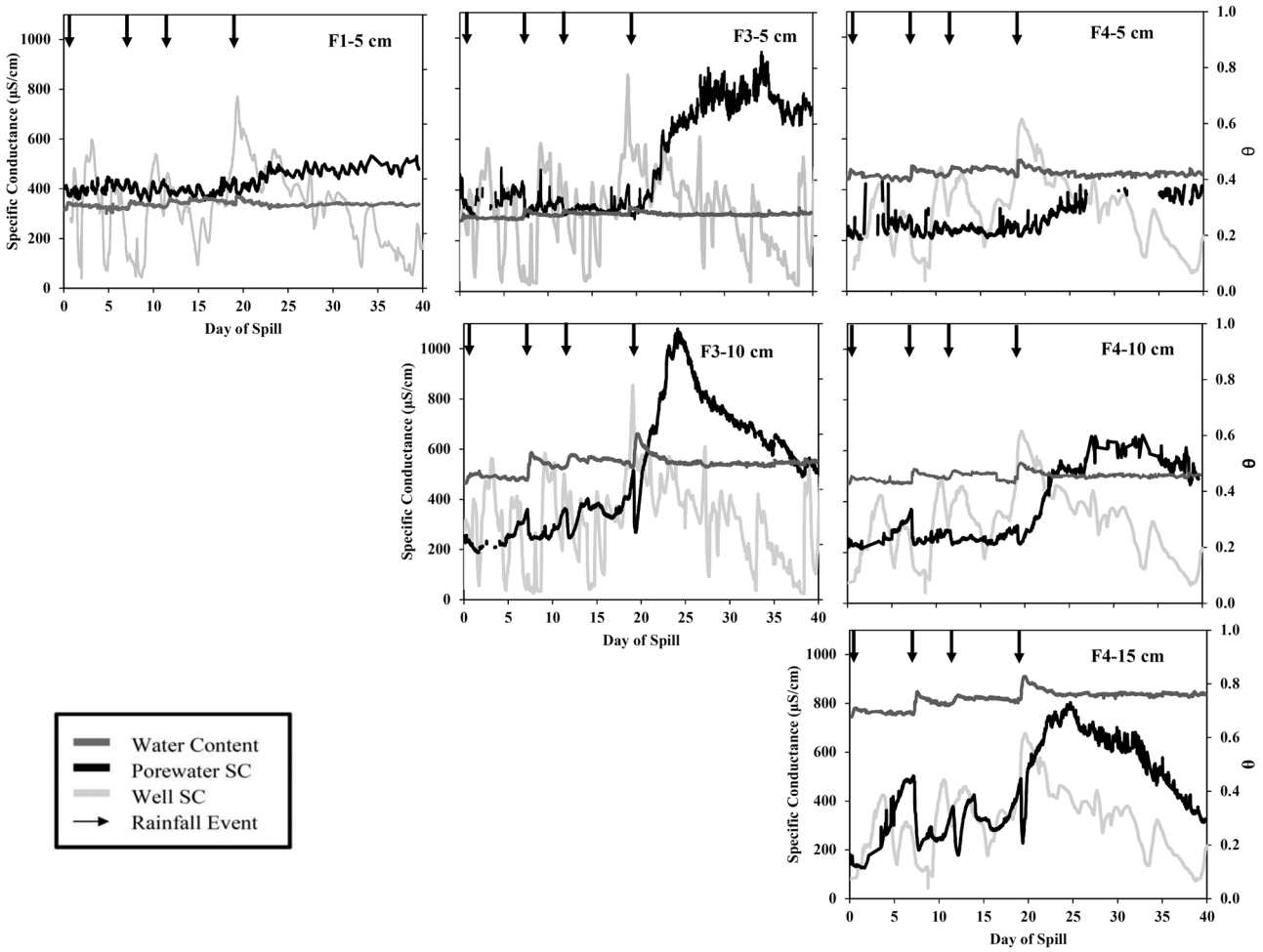


**FIGURE 4** Water content (θ) for selected time domain reflectometry (TDR) probes (dark gray) and corresponding porewater specific conductance ($SC_{pw}$, black). Also shown is the paired well SC ($SC_w$, light gray) representing the saturated zone. Significant rain events are indicated with black arrows

Day 19, following which the water table was relatively high and stable (Figure 3), $SC_{pw}$ values increased to peak values at all probes over the following 5–10 d. The $SC_{pw}$ remained elevated in the 5-cm probes (500, 800, and 400 µS $cm^{-1}$ in F1-5, F3-5, and F4-5) but declined in the deeper probes from 1,100 to 500 µS $cm^{-1}$ in F3-10, 600 to 500 µS $cm^{-1}$ in F4-10, and 800 to 350 µS $cm^{-1}$ in F4-15.

### 3.2 | Unsaturated solute breakthrough experiment

Over the 66-d laboratory mesocosm experiment, relative humidity (34 ± 3%) and air temperature (26.5 ± 1.7 °C) remained stable. Evaporation rates from water pans placed at each of the four mesocosms showed little spatial variance; the cumulative difference between the pans with the highest and lowest evaporative rates was ~5% of the total evaporated depth of water. However, daily rates of evaporation differed between laboratory (L) mesocosms, with a total evaporative depth of 64, 127, 157, and 144 mm in mesocosms L1, L2, L3, and L4, respectively, over the 66-d period.

In mesocosms L1, L2, and L4, the measured θ and pressure head generally decreased over the duration of the experiment signaling hydrological non-steady-state conditions (Figure 5). Upwards pressure gradients between the 15- and 10-cm tensiometers ($i_{lower}$) and between the 10- and 5-cm depths ($i_{upper}$) were positive for the majority of the experiment (where measurable) in L1, L3, and L4. In L1 and L3, $i_{lower} > i_{upper}$, whereas in L4, $i_{lower} \approx i_{upper}$ and remained constant despite the decreasing θ. In L2, $i_{lower}$ decreased rapidly after Day 0 and was negative between Days 5 and 25. Due to instrument failure, $i_{upper}$ could not be measured. No evidence of suction loss (i.e., air entry at the tube–mesocosm interface) was observed between the 15- and 10-cm tensiometers, suggesting $i_{lower}$ was not due to instrument failure.

Porewater $Cl^-$ and $Na^+$ concentrations increased above background values on Days 21,15, and 12 in mesocosms L1, L2, and L3, respectively (Figure 6), corresponding to the rates of water rise driven by evaporation in each core. Chloride concentrations generally decreased with height and increased over time, except for in mesocosm L3, in which concentrations plateaued after Day 50 (Figure 6). Breakthrough of $Cl^-$ (50% of the input concentration of $Cl^-$ [$C_{Cl,in}$] = 91 mg $L^{-1}$) was reached at the 5-cm depth in mesocosms L2 and L3 on Days 42 and 48, respectively, but was not achieved in mesocosm L1, which only experienced breakthrough at the 15-cm depth at Day 66 (the last day of the experiment). Due to the inability to collect samples at L1-10 cm and the inconsistency of SC–ion relationships in this layer, concentrations in this layer are unknown. The increase in $Na^+$ concentration occurred at a rate ~0.45 times that of $Cl^-$ at all mesocosms over all depths, though patterns of increase were consistent with $Cl^-$ (Figure 6). Breakthrough of $Na^+$ (50% of the input concentration of $Na^+$ [$C_{Na,in}$] = 59 mg $L^{-1}$) only reached the 10-cm depth in mesocosm L2 on Day 66 and did not occur at either sampled depth in mesocosm L1.

### 3.3 | Physical soil properties

Generally, in each mesocosm dry bulk density ($\rho_d$) was the lowest (Figure 7) and specific yield ($S_y$), total porosity ($n_t$), and effective porosity ($n_e$) were the highest in the top 5 cm. The $\rho_d$ increased while $n_t$ and $n_e$ decreased up to a depth of 15 cm bgs, after which the trend gently reversed with increasing depth. The change in $S_y$ was less pronounced, remaining relatively constant within the top 15 cm; the exception was L2B and L1B, in which $S_y$ was the highest at 5 cm and decreased rapidly with depth in the top 10–15 cm. Thereafter, $S_y$ increased slightly to the bottom of each core. Heterogeneity was pronounced in the top 15 cm, and the ranges of values for all physical parameters were often as large within a single mesocosm's subcores as they were between mesocosms. During laboratory analysis, a distinct root network was observed in cores L1A and L1B; depths where roots were found had both a larger bulk density and a larger porosity than the paired core without roots present (Figure 7).

The water retention experiments showed a high degree of variability between and within mesocosms in the top 15 cm (Figure 8). Generally, slices with a higher $\rho_d$ and a lower $n_e$ and $S_y$ at a given depth, such as L1A 0–5 cm, L3A 5–10 cm, and L3A and B 10–15 cm, had a greater water retention during drainage (decreasing θ, Figure 8). Water retention generally increased with depth to 20–25 cm bgs and plateaued or decreased below this. The $K_{unsat}$ ($5 \times 10^{-8}$ to $5 \times 10^{-7}$ m $s^{-1}$) was three to four orders of magnitude lower than $K_{sat}$ in all cores and displayed little variation with pressure once desaturated.

Pore fraction distributions showed a general increase in the smallest pores (<20 µm) by ~30% and a decrease in the largest pores (>386 µm) by ~10% between the surface and 15–20 cm bgs; below this, the number of pores <20 µm decreased by up to 20%, and pores >386 µm increased by ~5%. Pores between 77 and 386 µm varied the least with depth and within and between mesocosms, whereas pores in the 20–77 µm varied by up to 20% between cores and depths but did not show a consistent trend with depth.

## 4 | DISCUSSION

### 4.1 | Field experiment

The water contents (θ) at the "saturated" probes; Hummock F1-10 cm (F1-10), F1-15, F2-5, F2-10, F2-15, and F3-15

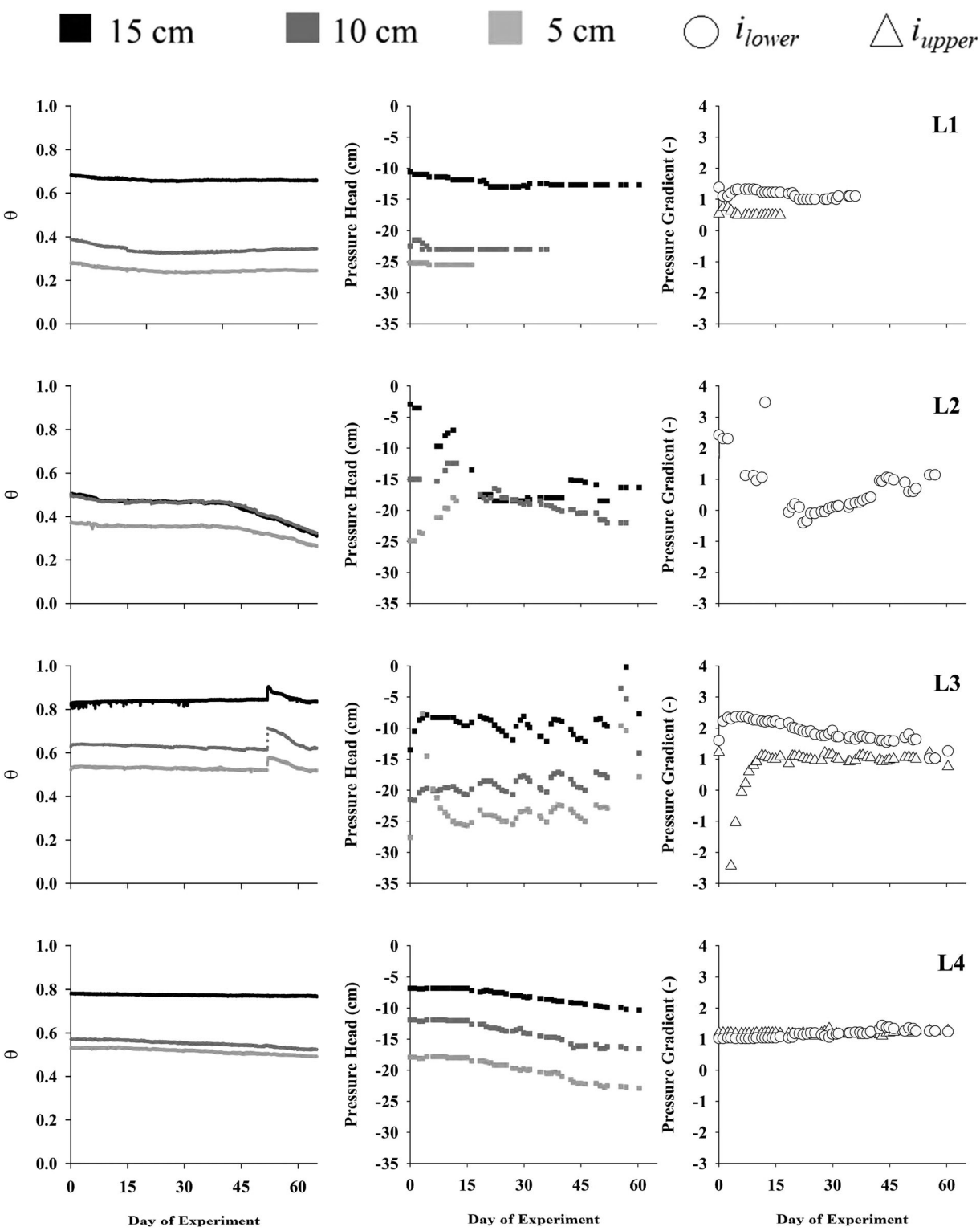


**FIGURE 5** Water content (θ) (left), pressure head (center), and pressure gradient (right, between the 15- and 10-cm tensiometers [$i_{\text{lower}}$] and between the 10- and 5-cm depths [$i_{\text{upper}}$]) data for mesocosms L1–L4 throughout experiment duration

(not shown) were within the expected range of total porosity of northern Canadian *Sphagnum* peat (0.85–0.99) (Carey, Quinton, & Goeller, 2007; McCarter et al., 2018; Rezanezhad et al., 2010) for the respective depths, reflecting their position at or below the water table. Each partially saturated hummock responded uniquely in both saturated and unsaturated zones due to unique depth dependent properties, the differing heights above water table (awt), and the general wetting

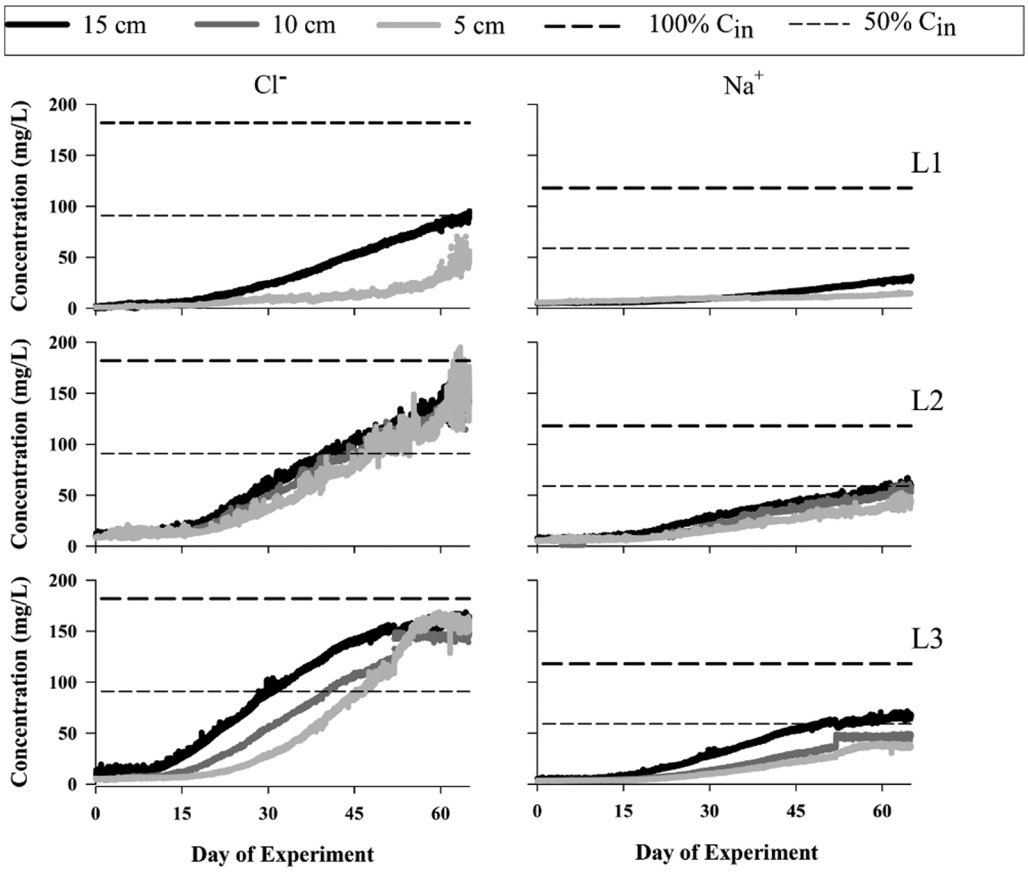


**FIGURE 6** Chloride and $Na^+$ concentration at the 5-, 10-, and 15-cm depths at mesocosm L1–L3. Mesocosm L4 was not included, as all anion and cation concentrations remained <5 mg $L^{-1}$. Dashed lines indicate the input concentration ($Cl_{in}$)

that occurred from the start of the spill to Day 19. In all three hummocks, there appears to be hysteresis with higher θ noted at all depths after Day 19 at equivalent water table depths, suggesting this wetting event may have saturated larger pores, switching from the wetting curve to the drying curve (Price & Whittington, 2010). This is also reflected below the water table, in which rain events prior to Day 19 decreased $SC_w$, likely due to dilution, whereas rainfall events on and after Day 19 resulted in $SC_w$ spikes due to an increased lateral connection with source $SC_w$ (Supplemental Figure S1).

The surface of hummock F1 at the F1-5 probe was the closest of all probes to the water table (0–9 cm awt) but had the lowest θ and minimal $SC_{pw}$ rise, which remained elevated after plateauing at around Day 23 (Figures 3 and 4). The low θ suggests that at this depth, there is a predominance of loosely structured moss with large pore sizes, which have a high $K_{sat}$ and low water retention. This transmitted water well during saturated conditions, as shown by the lack of water table rise above 5 cm bgs during precipitation events (Figure 3), as water readily drains away. In unsaturated conditions, the low water retention at F1-5 restricts upward movement of water (Gauthier et al., 2018; McCarter & Price, 2014), only facilitating capillary rise from the water table during its peak on Day 19 (Figure 3, θ = 0.3); this corresponds to the only notable increase in $SC_{pw}$ at this location. The relatively low water content suggests that only the smaller pores remained saturated after this, and the steady $SC_{pw}$ suggests these remained isolated for the duration of the experiment (Figure 4).

The surface of hummock F3 was of intermediate height awt; the deepest unsaturated probe F3-10 was 5–11 cm awt. Near-surface moss in F3 appears to have a higher water retention and better facilitated upward unsaturated water movement than at F1, as shown by the greater θ, larger increases in $SC_{pw}$, and the decline of $SC_{pw}$ during rainfall events (Figure 4) compared with the F1 0–5 probe, which was closer to the water table.

The surface of hummock F4 was the highest awt, the deepest unsaturated probe (F4-15) was 2–14 cm awt, and the shallowest F4-5 was 11–24 cm awt (Figures 3 and 4). Peat here has the highest water retention, as the shallowest probe F4-5 (11–24 cm awt) has a ~10% higher water content than F3-5 and F1-5, although the latter were consistently ~6 and ~13 cm closer to the water table, respectively. While maintaining a higher θ, the near-surface peat of hummock F4 appeared disconnected from the saturated zone; similar to F1-5, $SC_{pw}$ increased minimally before Day 19 and increased for a short period (<5 d)

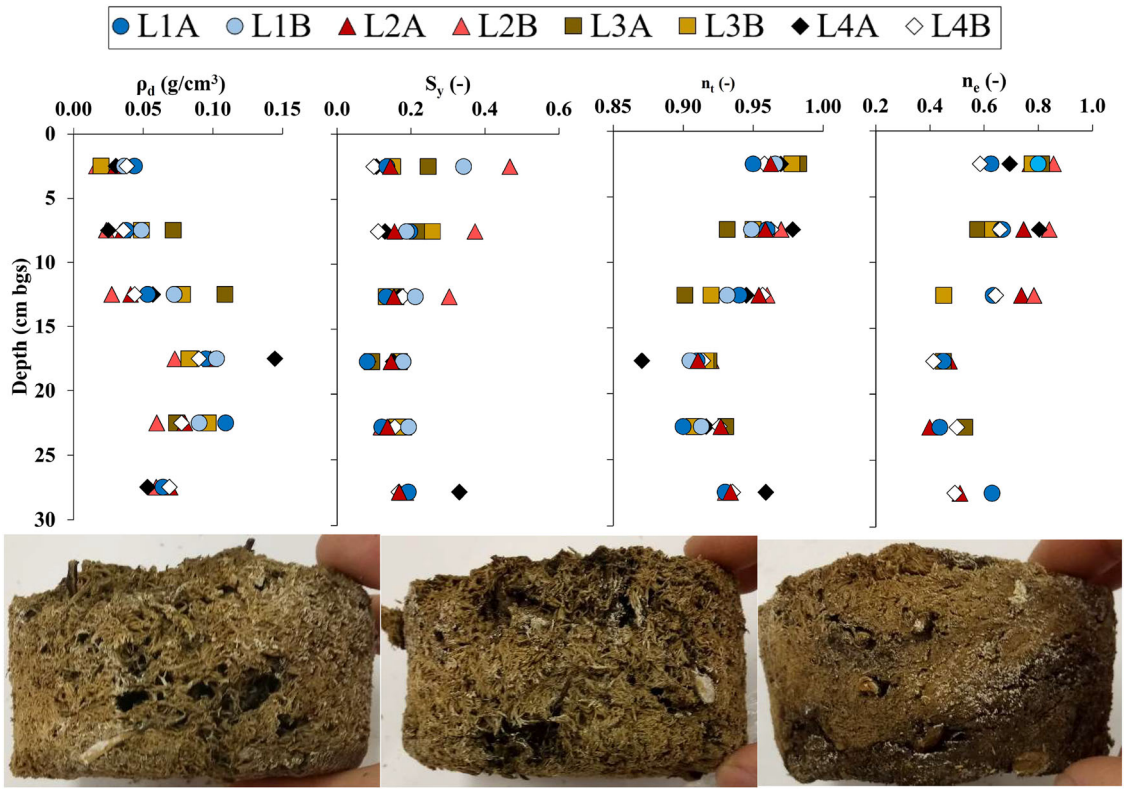


**FIGURE 7** Soil dry bulk density ($\rho_d$, top far left), specific yield ($S_y$, middle left), total porosity ($n_t$, middle right), and effective porosity ($n_e$, far right) measurements for mesocosms L1–L4 taken from duplicate 5-cm slices. Unique soil structure observed in mesocosm L1 during soil parameter analysis, featuring a dense root associated with large voids in L1B 0–5 cm (bottom left) and L1A 5–10 cm (bottom middle) and smaller voids in L1B 20–25 (bottom right). bgs, below ground surface

at Day 19 before stabilizing to the end of the spill. At greater depths (F4-10 and F4-15), capillary rise appeared well facilitated, as shown by the large increase in SC above the water table, and the faster decline of SC that corresponded to the decrease of saturated zone $SC_w$ towards the end of the spill.

## 4.2 | Unsaturated solute breakthrough experiment

Despite the close proximity of mesocosms when sampling, the soil physical properties showed a large range between and within mesocosms, underscoring the high spatial variability in natural systems (McCarter et al., 2014; Rezanezhad et al., 2016; Siegel & Glaser, 2006). Despite this variability, soil parameters fell within expected ranges of northern Canadian *Sphagnum* peat, including bulk density (Bunbury, Finkelstein, & Bollmann, 2012; McCarter et al., 2018), total porosity (Carey et al., 2007; McCarter et al., 2018; Rezanezhad et al., 2010), and effective porosity (Carey et al., 2007; McCarter et al., 2018; Rezanezhad et al., 2010). Although no geographically close data were available, θ or $K_{unsat}$ vs. pressure relationships were within other published values (Carey et al., 2007; Gnatowski, Szatyłowicz, Brandyk, & Kechavarzi, 2010; Price & Whittington, 2010; Rezanezhad et al., 2010). The pattern of increasing bulk density and decreasing total and effective porosity with depth in cores above the 15- to 20-cm depth was expected (Hayward & Clymo, 1982; McCarter & Price, 2014; Price et al., 2008); however, the steadying or slight reversal of these parameters below this depth was unexpected. The reversal may be attributable to the presence of other vegetation such as roots and woody debris, which is known to change layering and pore structure (Rezanezhad et al., 2016), or could be a layer of lesser decomposed *Sphagnum*, an artifact of historical conditions that favored rapid growth and wetting in this region (Glaser, Hansen, Siegel, Reeve, & Morin, 2004; Riley, 2011).

The unique hydrological and solute transport observations driven by evaporation at each mesocosm reflects differences in their hydraulic and physical character (open water evaporation at each location was similar). The net decrease in θ and pore water pressure over time reflects the extended time it takes for a large, relatively wet sample to come to equilibrium, as is demonstrated by the relatively flat tails of the drainage curves (Figure 8).

Mesocosm L1 exhibited the lowest rate of evaporation (1.0 mm $d^{-1}$), the slowest increase in solute concentration (Figure 6), and the lowest θ at all depths (Figure 5). The

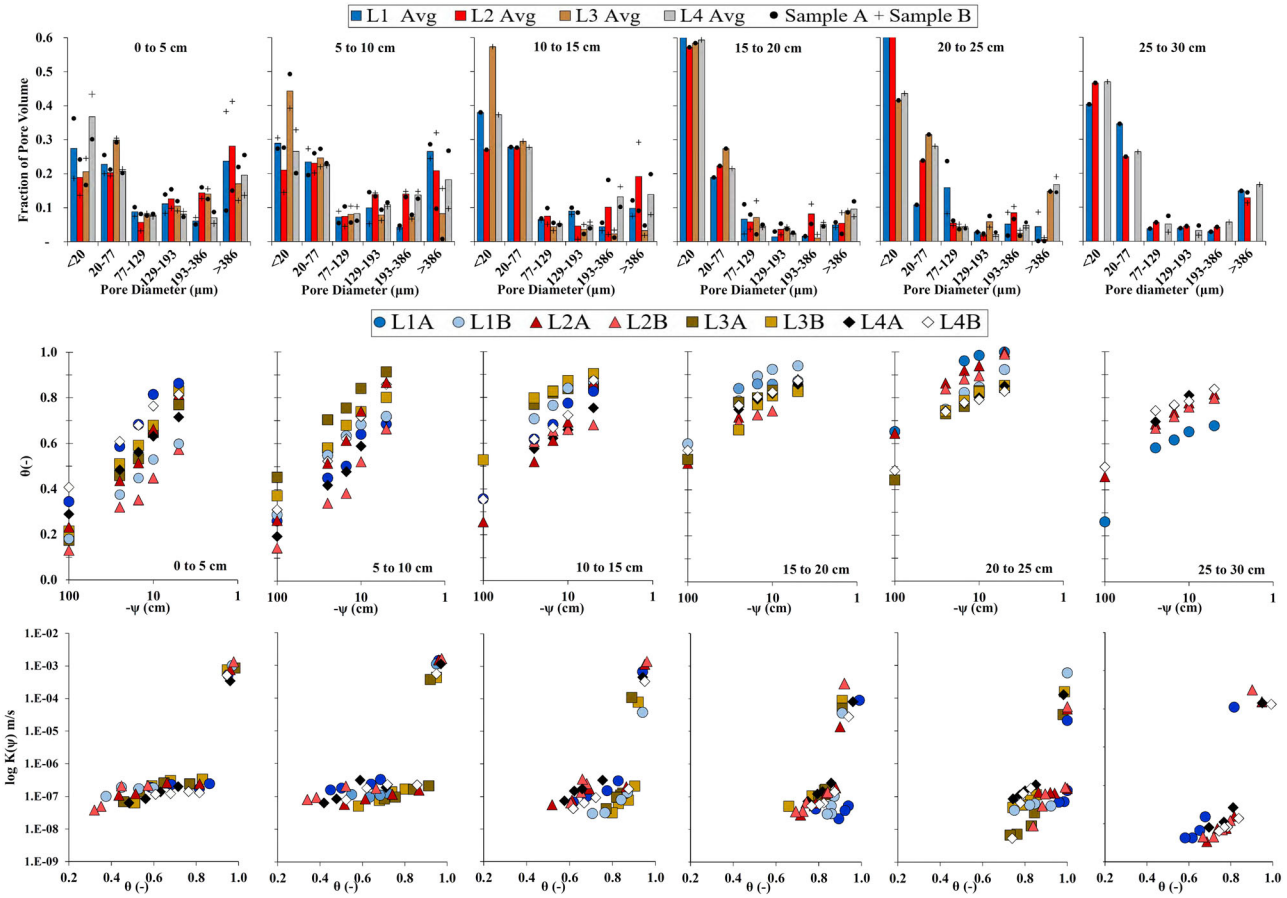


**FIGURE 8** Pore size distribution (top) including average (bar) and individual slices (x's and circles), water content (θ) as a function of negative porewater pressure (−ψ, middle), and unsaturated hydraulic conductivity as a function of water content (bottom) for mesocosms L1–L4

hydrophysical structure and behavior of this mesocosm appears to be disrupted by a complex root system found intermittently within the subcores (Figure 7). The lower $\rho_d$ and higher $S_y$, $n_t$, and $n_e$ in 0–5 cm L1B compared with L1A corresponds to an abundance of >386-µm-diam. pores in L1B and is consistent with a void-filled root network found only in the L1B slice (Figure 7). The low water retention in L1B (Figure 8) corresponds to the low θ observed in the laboratory, in spite of the high water retention of paired subcore L1A, suggesting that the properties of the mesocosm as a whole are not reflected in the properties of L1A. At greater depths, where the root network was observed in once slice (L1A 5–10, L1B 20–25) corresponding to a lower density and higher porosity there, is consistently a larger proportion of large (>386 um) pores than in the other subslice at the same depth, where the root network was absent. It appears that the root network has resulted in poor connectivity between depths in this core. However, the mechanisms causing this are likely complex and warrant further investigation at future sites.

Mesocosm L2 experienced an average rate of evaporation of (2.0 mm $d^{-1}$), $Cl^-$ breakthrough at all three depths by Day 48, and $Na^+$ breakthrough by the end of the experiment at 10 and 15 cm (Figure 6). The large decline in θ, and decrease or reversal of hydraulic gradient due to similar θ at the 15- and 10-cm intervals (Figure 5) are a product of mesocosm structure. Subcore L2B is consistently the least dense and most porous of all slices for each depth in the top 15 cm (Figure 8), corresponding to an abundance of pores >386 µm, which conduct water well in the saturated zone but drain quickly above the water table (Figure 8), limiting evaporation and thus solute rise. It is likely that the observed water content and solute uplift in the breakthrough experiment would be lower if not for the moderating effect of peat within this mesocosm corresponding to properties measured in L2A, which displayed lower fractions of pores >386 µm and high fractions of pores 20–77 µm, higher water retention, and thus greater observed $K_{unsat}$ and capillary rise potential.

Mesocosm L3 experienced the highest rate of evaporation (2.4 mm $d^{-1}$), fastest breakthrough of $Cl^-$ and $Na^+$ (Figure 6), and the highest θ at all depths (Figure 5). The plateau in $Na^+$ and $Cl^-$ at Days 55–65 is likely due to the instrument failure on Day 50, which disrupted the hydraulic gradient between the 15- and 10-cm depths. The physical structure of the top 15 cm of mesocosm L3 appears to have created the most

"ideal" conditions of the three mesocosms for evaporation and thus solute accumulation (Figure 7). In the top 15 cm, both subcores have the largest fraction of pores 20–77 μm, but a low amount of pores >386 μm (Figure 8), resulting in both a high water retention and high $n_e$. Although $K_{unsat}$ is relatively low for a given θ, the higher θ maintained in this core compared with the other mesocosms allows for greater pore connectivity and effective capillary rise.

Although not directly observed, the long-term process of evapoconcentration may become important, particularly in the upper 5 cm of the mesocosms during extended dry periods. This behavior was recorded in the unsaturated column experiment using homogenized peat by Simhayov et al. (2018), where near-surface concentrations were greater than input concentrations by Day 120, where the water table was held 23 cm below the surface. In a field setting, a rain-free period of this duration is unlikely. Furthermore, the gradation of pore sizes present in undisturbed vs. homogenized peat would likely limit solute accumulation by evapoconcentration. The role of juxtaposing hydraulic parameters of different magnitude should be more systematically explored with a numerical model.

### 4.3 | Relations between field and laboratory results

Relationships obtained through the controlled conditions and detailed analysis of the laboratory experiment can be used as a point of comparison with field values. In both the field environment and in laboratory mesocosms, the high variability of hydraulic and physical properties within and between peat profiles resulted in distinctly different hydraulic and thus solute transport and distribution behaviors. This highlights the importance of recognizing and accounting for significant heterogeneity when attempting to quantify processes using a finite number of samples (Carey et al., 2007; Goetz & Price, 2015; McCarter & Price, 2014; Rezanezhad et al., 2010). Under field conditions, the antecedent state and ongoing climatic events further influence the upward mobility and retention of solute.

In both laboratory and field experiments, the presence of high-porosity peat at the surface has the potential to facilitate or limit upwards solute mobility, depending on water retention capacity. If the water retention capacity of the uppermost layer is low, it renders it somewhat independent of distance to water table, as evidenced by the similarly low θ in hummock F2-5 (5 cm above the average water table) and F4-5 (18 cm above the water table). However, the structure of the peat profile must be considered. Low θ and low evaporation losses can result from loose and porous surficial peat with an abundance of large pores (mesocosm L2). However, high θ and evaporation losses were observed when highly porous surficial peat contains an abundance of small but connected pores (i.e., ~20–77 μM), which allows the peat to maintain sufficient water retention capacity to supply water to the surface. These relationships can be further complicated by the presence of vascular vegetation, the roots of which can disrupt the structure of the peat profile and limit unsaturated pore connectivity (mesocosm L1).

### 4.4 | Limitations

In the field experiment, SC was used as a surrogate measure of NaCl presence rather than direct sampling. It is likely that the added $Na^+$ and $Cl^-$ ions were the dominant contributor to porewater SC due to the relatively low concentrations of other anions and cations in the laboratory-tested peat.

Despite the precautions taken to ensure undisturbed extraction and shipping of peat mesocosms, it is likely that some loss of original structure occurred during transportation. Prior to the start of the experiment, each mesocosm experienced additional subsidence in the amount of 5–7 cm during the 60-d settling period, suggesting an additional breakdown of the original pore structure. This would be problematic if parameters derived from these mesocosms were being used to drive simulations of field conditions, but this was not done here. All measured soil parameters were extremely sensitive to small changes in slice structure and weight, due to the small size of soil samples being tested.

The small sample size of cores ($n = 4$) combined with the large amount of observed heterogeneity suggests that the full scale of potential behavioral variability may not have been captured with this experiment. More intensive sampling or parameter modeling will aid in further characterization. This could be investigated further by performing a sensitivity analysis using a one-dimensional approximation of the Richard's equation, such as with Hydrus 1D (McCarter & Price, 2014).

## 5 | SUMMARY AND CONCLUSIONS

Characterization of unsaturated zone solute behavior faces several unique challenges at both field and laboratory scales. At the field scale, saturated zone processes and hydrological conditions have a strong influence on the presence and amount of solute above the water table. Rainfall events, and a subsequent rise in water table elevation, increased connectivity between unsaturated hummocks and the saturated zone. Near the surface where peat has low water retention, solute concentrations may then remain elevated after post-rainfall drainage.

In controlled laboratory conditions, inter- and intra-mesocosm heterogeneity results in highly varied hydrological and solute behavior. The 50% breakthrough of $Cl^-$ occurred at all depths in two of three mesocosms in an unsaturated

breakthrough experiment, whereas 50% breakthrough of $Na^+$ only occurred at the 15-cm depth in two of three mesocosms. Mesocosms that experienced breakthrough had higher rates of evaporation and thus solute uplift. The highest evaporative and upward solute flux was seen in the mesocosm, which had a high effective porosity but relative paucity of large (>386 μm) pores at the 0- to 5-cm depth, underlain by much denser, less porous peat, which could supply solute and increase the θ above it.

Measured physical parameters of mesocosms fell within ranges specified by previous studies; however, a less common decrease in bulk density and increase in total and effective porosity was noted in depths below 15 cm for all mesocosms. This is likely due to the presence of other vegetation or due to less decomposed peat at depth. A complex vascular root network was also present within the L1 mesocosm, which disrupted depth-dependent progression of physical parameters and appeared to limit solute rise.

The long-term effect of evapoconcentration was not observed during the field experiment due to wet conditions, or in the laboratory experiment due to the limited time of the experiment (66 d). It is likely that under drier conditions and longer time scales, evapoconcentration would play a more significant role in solute concentrations. However, given the 66-d experiment with zero recharge or flushing from above, it seems likely that rain events in a field setting could limit the accumulation of solutes in the top part of the profile.

Observed increases in porosity and decreases in bulk density below 15 cm draws attention to potential error in assuming linear or exponentially increasing patterns with depth. Interactions between layers of changing mesocosm structure, as well as an understanding of pore size distribution, were determined to be paramount in understanding solute transport mechanisms, creating the need for detailed parameterization in near-surface (acrotelm) peat when developing vadose zone models. Further, care should be taken when assuming extracted mesocosms are representative of site conditions, as even mesocosms taken within visually similar areas had markedly different solute transport behaviors in both laboratory and field conditions. Subcores extracted from these mesocosms may also show nonrepresentative behavior where peat structure is complex, particularly where vascular vegetation is present. Further analysis of hollow and lawn microtopography will confirm if similar caution should be used for other microtopes.

Conclusions from this research demonstrate the potential for solute to accumulate and become entrapped in near-surface peat in a complex and heterogenous manner, highlighting the susceptibility of surficial mosses and vegetation to subsurface contaminant spills. To better understand and accurately assess and mitigate potential spill impacts, there is a need for detailed near-surface parameterization and incorporation of these processes into unsaturated zone solute transport models.

## CONFLICT OF INTEREST

The authors declare no conflict of interest.

## ACKNOWLEDGMENTS

The authors would like to acknowledge funding from the Canadian Network for Aquatic Ecosystem Services and an Natural Science and Engineering Research Council Discovery Grant to J.S. Price. We would also like to thank the De Beers Group of Companies Victor Diamond Mine staff, in particular the Environment Department, for their ongoing assistance and hospitality. We would like to thank Colin McCarter, Rubi Simhayov, and James Sherwood for their technical support.

## ORCID

*Nicole E. Balliston*
https://orcid.org/0000-0003-4765-328X

## REFERENCES

Baird, A. J., & Gaffney, S. W. (2000). Solute movement in drained fen peat: A field tracer study in a Somerset (UK) wetland. *Hydrological Processes*, *14*, 2489–2503. https://doi.org/10.1002/1099-1085(20001015)14:14⟨2489:AID-HYP110⟩3.0.CO;2-Q

Balliston, N. E., McCarter, C. P., & Price, J. S. (2018). Microtopographical and hydrophysical controls on subsurface flow and solute transport: A continuous solute release in a subarctic bog. *Hydrological Processes*, *32*, 2963–2975. https://doi.org/10.1002/hyp.13236

Bear, J. (1972). *Dynamics of fluids in porous materials*. Society of Petroleum Engineers.

Bunbury, J., Finkelstein, S., & Bollmann, J. (2012). Holocene hydroclimatic change and effects on carbon accumulation inferred from a peat bog in the Attawapiskat River watershed, Hudson Bay lowlands, Canada. *Quaternary Research*, *78*, 275–284. https://doi.org/10.1016/j.yqres.2012.05.013

Carey, S. K., Quinton, W. L., & Goeller, N. T. (2007). Field and laboratory estimates of pore size properties and hydraulic characteristics for sub-arctic organic soils. *Hydrological Processes*, *21*, 2560–2571. http://doi.org/10.1002/hyp.6795

Dobson, R., Schroth, M. H., & Zeyer, J. (2007). Effect of water-table fluctuation on dissolution and biodegradation of a multi-component, light nonaqueous-phase liquid. *Journal of Contaminant Hydrology*, *94*, 235–248. https://doi.org/10.1016/j.jconhyd.2007.07.007

Environment Canada. (2015a). *Canadian climate normals 1971–2000: Lansdowne House*. Environment Canada. Retrieved from http://www.climate.weatheroffice.gc.ca/climate_normals/

Environment Canada. (2015b). *Canadian climate normals 1971–2000: Moosonee*. Environment Canada. Retrieved from http://www.climate.weatheroffice.gc.ca/climate_normals/

Gauthier, T.-L., McCarter, C. P. R., & Price, J. S. (2018). The effect of compression on *Sphagnum* hydrophysical properties: Implications for increasing hydrophysical connectivity in restored cutover peatlands. *Ecohydrology.*, *11*(8). https://doi.org/10.1002/eco.2020

Gharedaghloo, B., & Price, J. S. (2018). *Characterizing the transport of hydrocarbon contaminants in peat soils and peatlands (Doctoral dissertation)*. Waterloo, ON, Canada: University of Waterloo.

Glaser, P. H., Hansen, B. C., Siegel, D. I., Reeve, A. S., & Morin, P. J. (2004). Rates, pathways and drivers for peatland development in the Hudson Bay lowlands, northern Ontario, Canada. *Journal of Ecology*, *92*, 1036–1053. https://doi.org/10.1111/j.0022-0477.2004.00931.x

Gnatowski, T., Szatyłowicz, J., Brandyk, T., & Kechavarzi, C. (2010). Hydraulic properties of fen peat soils in Poland. *Geoderma*, *154*, 188–195. http://doi.org/10.1016/j.geoderma.2009.02.021

Goetz, J. D., & Price, J. S. (2015). Role of morphological structure and layering of *Sphagnum* and *Tomenthypnum* mosses on moss productivity and evaporation rates. *Canadian Journal of Soil Science*, *95*, 109–124. https://doi.org/10.4141/cjss-2014-092

Hayward, P. M., & Clymo, R. S. (1982). Profiles of water content and pore size in *Sphagnum* and peat, and their relation to peat bog ecology. *Proceedings of the Royal Society B: Biological Sciences*, *215*, 299–325. http://doi.org/10.1098/rspb.1982.0044

Hilhorst, M. A. (2000). A pore water conductivity sensor. *Soil Science Society of America Journal*, *64*, 1922–1925. https://doi.org/10.2136/sssaj2000.6461922x

Hoag, S. R., & Price, J. S. (1997). The effects of matrix diffusion on solute transport and retardation in undisturbed peat in laboratory columns. *Journal of Contaminant Hydrology*, *28*, 193–205. https://doi.org/10.1016/S0169-7722(96)00085-X

Hoag, S. R., & Price, S. J. (1995). A field-scale, natural gradient solute transport experiment in peat at a Newfoundland blanket bog. *Journal of Hydrology*, *172*, 171–184. http://doi.org/10.1016/0022-1694(95)02696-M

Ingram, H. A. P. (1978). Soil layers in mires: Function and terminology. *European Journal of Soil Science*, *29*, 224–227. http://doi.org/10.1111/j.1365-2389.1978.tb02053.x

Kellner, E., & Lundin, L. C. (2001). Calibration of time domain reflectometry for water content in peat soil. *Hydrology Research*, *32*, 315–332. https://doi.org/10.2166/nh.2001.0018

Lewis, A. M. (1988). A test of the air-seeding hypotehesis using *Sphagnum* hyalocysts. *Plant Physiology*, *87*, 577–582. https://doi.org/10.1104/pp.87.3.577

McCarter, C. P. R., & Price, J. S. (2017a). Experimental hydrological forcing to illustrate water flow processes of a subarctic ladder fen peatland. *Hydrological Process*, *31*, 1578–1589. https://doi.org/10.1002/hyp.11127

McCarter, C. P. R., & Price, J. S. (2017b). The transport dynamics of chloride and sodium in a ladder fen during a continuous wastewater polishing experiment. *Journal of Hydrology*, *549*, 558–570. https://doi.org/10.1016/j.jhydrol.2017.04.033

McCarter, C. P. R., Rezanezhad, F., Gharedaghloo, B., Price, J. S., & Van Cappellen, P. (2019). Transport of chloride and deuterated water in peat: The role of anion exclusion, diffusion, and anion adsorption in a dual porosity organic media. *Journal of Contaminant Hydrology*, *225*. https://doi.org/10.1016/j.jconhyd.2019.103497

McCarter, C. P. R., Weber, T. K., & Price, J. S. (2018). Competitive transport processes of chloride, sodium, potassium and ammonium in fen peat. *Journal of Contaminant Hydrology*, *217*, 17–31. https://doi.org/10.1016/j.jconhyd.2018.08.004

McCarter, C. P., & Price, J. S. (2014). Ecohydrology of *Sphagnum* moss hummocks: Mechanisms of capitula water supply and simulated effects of evaporation. *Ecohydrology*, *7*, 33–44. https://doi.org/10.1002/eco.1313

Nungesser, M. K. (2003). Modelling microtopography in boreal peatlands: Hummocks and hollows. *Ecological Modelling*, *165*, 175–207. http://doi.org/10.1016/S0304-3800(03)00067-X

Ours, D. P., Siegel, D. I., & Glaser, P. H. (1997). Chemical dilation and the dual porosity of humified bog peat. *Journal of Hydrology*, *196*, 348–360. http://doi.org/10.1016/S0022-1694(96)03247-7

Pouliot, R., Rochefort, L., & Graf, M. D. (2012). Impacts of oil sands process water on fen plants: Implications for plant selection in required reclamation projects. *Environmental Pollution*, *167*, 132–137. http://doi.org/10.1016/j.envpol.2012.03.050

Price, J. S., & Whittington, P. N. (2010). Water flow in *Sphagnum* hummocks: Mesocosm measurements and modelling. *Journal of Hydrology*, *381*, 333–340. http://doi.org/10.1016/j.jhydrol.2009.12.006

Price, J. S., Whittington, P. N., Elrick, D. E., Strack, M., Brunet, N., & Faux, E. (2008). A method to determine unsaturated hydraulic conductivity in living and undecomposed *Sphagnum* moss. *Soil Science Society of America Journal*, *72*, 487–491. http://doi.org/10.2136/sssaj2007.0111N

Price, S. J., & Woo, M. K. (1986). Wetlands as waste repositories?: Solute transport in peat. In *Proceedings of the National Student Conference on Northern Studies* (pp. 18–19). Ottawa: Association of Canadian Universities for Northern Studies.

Quinton, W. L., Elliot, T., Price, J. S., Rezanezhad, F., & Heck, R. (2009). Measuring physical and hydraulic properties of peat from X-ray tomography. *Geoderma*, *153*, 269–277. http://doi.org/10.1016/j.geoderma.2009.08.010

Rezanezhad, F., Price, J. S., & Craig, J. R. (2012). The effects of dual porosity on transport and retardation in peat: A laboratory experiment. *Canadian Journal of Soil Science*, *92*, 723–732. http://doi.org/10.4141/cjss2011-050

Rezanezhad, F., Price, J. S., Quinton, W. L., Lennartz, B., Milojevic, T., & Van Cappellen, P. (2016). Structure of peat soils and implications for water storage, flow and solute transport: A review update for geochemists. *Chemical Geology*, *429*, 75–84. https://doi.org/10.1016/j.chemgeo.2016.03.010

Rezanezhad, F., Quinton, W. L., Price, J. S., Elliot, T. R., Elrick, D., & Shook, K. R. (2010). Influence of pore size and geometry on peat unsaturated hydraulic conductivity computed from 3D computed tomography image analysis. *Hydrological Processes*, *24*, 2983–2994. http://doi.org/10.1002/hyp.7709

Riley, J. L. (2011). *Wetlands of the Ontario Hudson Bay lowland: A regional overview*. Toronto, ON, Canada: Nature Conservancy of Canada.

Ronkanen, A. K., & Kløve, B. (2007). Use of stabile isotopes and tracers to detect preferential flow patterns in a peatland treating municipal wastewater. *Journal of Hydrology*, *347*, 418–429. https://doi.org/10.1016/j.jhydrol.2007.09.029

Siegel, D. I., & Glaser, P. (2006). The hydrology of peatlands. In: R. K. Wieder & D. H. Vitt (Eds.), *Boreal peatland ecosystems* (pp. 289–311). Berlin, Heidelberg, Germany: Springer. https://doi.org/10.1007/978-3-540-31913-9_13

Simhayov, R. B., Weber, T. K., & Price, J. S. (2018). Saturated and unsaturated salt transport in peat from a constructed fen, *Soil*, *4*, 63–81. https://doi.org/10.5194/soil-4-63-2018

Steinback, B. (2012). *De Beers Canada Inc. Victor Mine northeast fen 2011 annual report per Condition 8(3) of Certificate of Approval no. 4056-6w8qbu*. Toronto, ON, Canada: De Beers Canada.

Waddington, J. M., Morris, P. J., Kettridge, N., Granath, G., Thompson, D. K., & Moore, P. A. (2015). Hydrological feedbacks in northern peatlands. *Ecohydrology*, *8*, 113–127. https://doi.org/10.1002/eco.1493

Weber, T. K., Iden, S. C., & Durner, W. (2017). Unsaturated hydraulic properties of *Sphagnum* moss and peat reveal trimodal pore-size distributions. *Water Resources Research*, *53*, 415–434. https://doi.org/10.1002/2016WR019707

Zoltai, S. C., & Kershaw, G. P. (1995). Large volume oil spill on land surface: The Vozey oil field, Russia. In *Proceedings of the Arctic and Marine Oil Spill Program Technical Seminar 2* (pp. 1177–1186.) Ottawa: Ministry of Supply and Services.

## SUPPORTING INFORMATION

Additional supporting information may be found online in the Supporting Information section at the end of the article.

**How to cite this article:** Balliston NE, Price JS. Heterogeneity of the peat profile and its role in unsaturated sodium chloride rise at field and laboratory scales. *Vadose Zone J*. 2020;19:e20015. https://doi.org/10.1002/vzj2.20015